THE JOURNAL OF BIOLOGICAL CHEMISTRY VOL. 288, NO. 39, pp. 28369–28381, September 27, 2013

Vitellogenin Recognizes Cell Damage through Membrane Binding and Shields Living Cells from Reactive Oxygen Species*

Received for publication, March 15, 2013, and in revised form, July 25, 2013 Published, JBC Papers in Press, July 28, 2013, DOI 10.1074/jbc.M113.465021

Heli Havukainen[‡§¶‖1], Daniel Münch[‡], Anne Baumann[§], Shi Zhong[¶], Øyvind Halskau[‡‡], Michelle Krogsgaard[¶], and Gro V. Amdam[‡**]**

*From the [‡]Department of Chemistry, Biotechnology, and Food Science, Norwegian University of Life Sciences, 1432 Aas, Norway, the [§]Department of Biomedicine, University of Bergen, Jonas Lies Vei 91, 5009 Bergen, Norway, the [¶]New York University Cancer Institute, New York University, New York, New York 10016, the [‖]Department of Biosciences, University of Helsinki, FIN-00014 Helsinki, Finland, the **School of Life Sciences, Arizona State University, Tempe, Arizona 85287-4501, and the [‡‡]Department of Molecular Biology, University of Bergen, Thormøhlensgate 55, 5020 Bergen, Norway*

Background: Vitellogenin is a central regulator of honey bee life span by largely unknown mechanisms.
Results: Honey bee vitellogenin has membrane affinity that is connected to cell damage recognition and antioxidant function.
Conclusion: Membrane binding documents a new molecular behavior among vitellogenins.
Significance: Vitellogenins are widespread phylogenetically, and their molecular behavior is essential for fitness traits in many animals.

Large lipid transfer proteins are involved in lipid transportation and diverse other molecular processes. These serum proteins include vitellogenins, which are egg yolk precursors and pathogen pattern recognition receptors, and apolipoprotein B, which is an anti-inflammatory cholesterol carrier. In the honey bee, vitellogenin acts as an antioxidant, and elevated vitellogenin titer is linked to prolonged life span in this animal. Here, we show that vitellogenin has cell and membrane binding activity and that it binds preferentially to dead and damaged cells. Vitellogenin binds directly to phosphatidylcholine liposomes and with higher affinity to liposomes containing phosphatidylserine, a lipid of the inner leaflet of cell membranes that is exposed in damaged cells. Vitellogenin binding to live cells, furthermore, improves cell oxidative stress tolerance. This study can shed more light on why large lipid transfer proteins have a well conserved α-helical domain, because we locate the lipid bilayer-binding ability of vitellogenin largely to this region. We suggest that recognition of cell damage and oxidation shield properties are two mechanisms that allow vitellogenin to extend honey bee life span.

Large lipid transfer proteins (LLTPs)[2] have multiple roles in animals; they are lipid transporters, inflammation suppressors, immunomodulators, and blood coagulators. Vitellogenin (Vg) is the ancient form of these proteins, with an estimated 700 million-year history (1). In most egg-laying species, Vg provides the eggs with lipids. Non-egg-laying vertebrates lack Vg but have homologs, such as apolipoprotein B (apoB), that transports cholesterol (2). Vgs are mostly produced in the liver or hepatopancreas (vertebrates, crustaceans) or fat tissue (insects), secreted into the blood, and taken up by targets, such as eggs, via receptor-mediated endocytosis (3, 4).

Many blood proteins are involved in innate immunity (for a review, see Ref. 5). They recognize pathogen-associated molecular patterns (PAMPs), such as lipopolysaccharides, or endogenous damage-associated molecular patterns (DAMPs), such as phosphatidylserine (PS) (6). Complement factors are perhaps the most studied group of these pattern recognition proteins (7). Also, collectins and pentraxins identify both PAMPs and DAMPs. They, among other targets, bind to membrane protrusions of damaged cells called blebs (8, 9). Like the LLTP family, Vg recognizes a variety of PAMPs and has antibacterial, antiviral, and antifungal effects studied in several fish, including salmon (*Salmo salar*) and zebrafish (*Danio rerio*) (10, 11). ApoB suppresses inflammation by neutralizing both PAMPs (12, 13) and necrotic cells (14). Broad-range danger recognition by individual proteins can be explained by their general affinity with exposed hydrophobic molecules and surfaces that many PAMPs and DAMPs consist of (6).

There is a conserved vitellogenin domain (Vg domain) located in the N terminus of LLTPs. The Vg domain has lipid affinity, and it appears to be important for the assembly of the lipoprotein complex (15, 16). The apoB Vg domain binds to egg phosphatidylcholine (PC) monolayers and dimyristoylphos-

* This work was supported, in whole or in part, by National Institutes of Health, NIA, Grant P01 AG22500. This work was also supported by Research Council of Norway Grants 180504, 185306, and 191699; the PEW Charitable Trust; and Norwegian Cancer Society Grant 58240001. The PROBE work was partly supported by the National Program for Research in Functional Genomics (FUGE) funded by the Norwegian Research Council.

[1] To whom correspondence should be addressed: Dept. of Chemistry, Biotechnology and Food Science, Norwegian University of Life Sciences, P.O. Box 5003, 1432 Aas, Norway. Tel.: 358-40-357-7977; Fax: 47-55586360; E-mail: hohavukainen@gmail.com.

[2] The abbreviations used are: LLTP, large lipid transfer protein; Vg, vitellogenin; apoB, apolipoprotein B; hlVg, vitellogenin purified from hemolymph; fbVg, vitellogenin purified from fat body; VgIR, Vg immunoreactivity; vWFD, von Willebrand factor D; PS, porcine brain phosphatidylserine; PC, egg yolk phosphatidylcholine; SPR, surface plasmon resonance; PAMP, pathogen-associated molecular pattern; ROS, reactive oxygen species; PI, propidium iodide; df, degree of freedom; HBS, Hepes-buffered saline.

phatidylcholine multilamellar vesicles that have been used in the studies of the apoB-lipid packing (15, 17), which takes place at the endoplasmic reticulum membrane. There is further evidence of direct binding of apoB to the epithelial cell membrane via the Vg domain (18), but the mechanisms and consequences of this cell binding are unclear. The Vg domain consists of two subdomains: the N-sheet domain and the α-helical domain. N-sheet alone has been identified as the Vg receptor-binding region in fish (19). The role of the α-helical domain is less clear. Outside of the Vg domain, all known Vgs (but not apoB) have a conserved but poorly characterized von Willebrand factor type D domain (vWFD) at their C terminus (3, 20).

LLTPs become easily oxidized in blood (for a review, see Ref. 21). Excessive oxidation of human apoB and its lipids is linked to atherosclerosis, which is an arterial response to chronic inflammation (22). In the honey bee (*Apis mellifera*), on the contrary, oxidative carbonylation of Vg is linked to beneficial effects. Vg titer positively correlates with the honey bee's oxidative stress tolerance, because the antioxidant property of Vg shields other hemolymph (the insect blood) molecules from reactive oxygen species (ROS) (23). According to the free radical theory of aging, the balance between ROS and antioxidants is essential in inhibition of chronic inflammation and aging-associated diseases (24). Generally, antioxidants include proteins that are located either in intra- or intercellular fluid or on membranes, where they can be permanently (25) or temporarily (26) attached.

Honey bee Vg appears to have also other life-extending effects. It supports immune cell viability (27) and suppresses risky foraging behavior performed by the essentially sterile helper (worker) bees of the colony (28). Excessive buildup of Vg (up to 100 mg/ml) in hemolymph is characteristic of an extremely long lived worker phenotype called winter bees that can survive at least 8 months, in contrast to the 4–8 weeks of a normal worker life span (29). Atypical changes in the workers' seasonal Vg expression can furthermore be used as an indicator of the disease syndrome colony collapse disorder, which in recent years has caused a dramatic loss of commercial honey bee populations worldwide (30).

Typically, honey bee Vg is a monomeric ~180-kDa protein, but the N-sheet of the Vg domain can dissociate in a probably phosphorylation-regulated process in fat tissue, leaving a 150-kDa putatively receptor-free Vg fragment remaining (31, 32). However, although honey bee Vg is a molecularly, physiologically, ecologically, evolutionarily, and commercially interesting protein, little is known about how this molecule confers its beneficial effects.

We hypothesized that affinity to hydrophobic surfaces, similarly to many serum proteins and the Vg domain in apoB, could be one of the shielding mechanisms of Vg in the honey bee. If this ROS scavenger protein had some affinity to the cell membrane, it could benefit cells under oxidative stress. On the other hand, affinity to DAMP-containing dying cells could link Vg to the anti-inflammatory function of apoB. To assess our hypothesis, we investigated Vg localization in honey bee tissues and the interaction of Vg with healthy, apoptotic, and dead insect cells. We also assayed Vg binding to membrane-mimicking PC and PS/PC bilayers. Vg was found to interact with tissues, cells, and bilayers, and the binding to dead cells and PS/PC was enhanced compared with healthy cells and PC. Furthermore, we used limited proteolysis, homology modeling, and tryptophan fluorescence to understand the binding mechanism and tested the potential of Vg to disrupt PS-liposomes. Finally, we tested whether Vg on the cell surface can affect the oxidative stress tolerance of live cells.

EXPERIMENTAL PROCEDURES

The Antibody, Gels, and Western Blots—The polyclonal Vg antibody produced in rabbit (Pacific Immunology, Ramona, CA) has been tested before (29, 31, 33). This antibody was used for all imaging and Western blotting. The gel and Western blot reagents were purchased from Bio-Rad. The Western protocol for all of the blots was as follows. The blotted nitrocellulose membrane was incubated with TBS containing 0.5% Tween with 2.5% fat-free milk powder overnight. The membrane was incubated for 1 h with the Vg antibody and for 1 h with a horseradish peroxidase-conjugated secondary antibody prior to imaging using an Immun-Star kit. All gels and blots were imaged, and band intensities were measured using a ChemiDoc XRS+ imager (Bio-Rad).

Material Sampling, Protein Purification, and Cell Lines—Handling of colony sources, honey bee tissue dissection, Vg extraction, and Vg purification was performed as described elsewhere (31). Single ion exchange purification was used for hemolymph vitellogenin (hlVg) purification. Fat body vitellogenin (fbVg) was purified from fat body protein extract (31) by GenScript with size exclusion chromatography and ion exchange steps (31), and the purification was completed with a Superdex 75 column (Sigma-Aldrich). The α-helical (residues 416–778) and vWFD (residues 1444–1615) domains were produced by GenScript; the vWFD DNA was subcloned into pUC57 vector, and the α-helical domain was subcloned into pCold trigger factor vector. The N-terminal hexahistidine tag of the fragments was used for one-step affinity purification. The α-helical domain is a fusion construct with trigger factor that is a highly soluble protein with chaperone activity (34), and separation of the α-helical fragment from its fusion partner by HRV 3C cleavage was not feasible due to fragmentation of the α-helical domain.

We used Sf9 or High Five cells in the *in vitro* experiments. Sf9 is a pupal *Spodoptera frugiperda* cell line, and High Five is a parental line of *Trichopulsia ni* (see provider's information; Invitrogen). Most experiments were performed with High Five cells due to their shorter doubling time.

Histology—Dissection, tissue preparation, and immunohistochemistry were largely performed as described previously (29). In brief, tissue samples of mature nest bees (age <27 days) were fixed in paraformaldehyde (4% in PBS), embedded in London Resin White (Electron Microscopy Science, Hatfield, PA), and cut with a Reichert Jung ultra-microtome (Leica, Wetzlar, Germany; section thickness, 1–2 μm). Mounted sections were rinsed with PBS-NTx (0.25% Triton X-100 in PBS), preincubated with 2% bovine serum albumin (BSA) (Sigma-Aldrich) in PBS-NTx for 60 min, and incubated overnight with the anti-Vg antibody (1:100). After washing in PBS-NTx, a Cy5-conjugated anti-rabbit antibody (Jackson ImmunoResearch, West Grove,

PA; 1:400) and the nuclear stain 4′,6-diamidino-2-phenylindole (DAPI; 1:1,000 from 0.5 mg/ml stock; Sigma-Aldrich) were co-applied. Finally, sections were rinsed in PBS-NTx and cleared in glycerol (30% in PBS). To rule out false positives, controls that were not incubated with the primary antibody were included. Two controls and two test samples were prepared for each of five individuals. Confocal images were acquired on a Leica TCS SP5 laser-scanning confocal microscope, using a ×63 oil immersion objective (numerical aperture = 1.4). Image stacks ($z = 2$ μm, $\Delta z = 0.5$ μm) or single optical sections (control *versus* test comparisons) were viewed and processed in ImageJ version 1.44b (National Institutes of Health).

Membrane Protein Immunoblot—The membrane protein extraction protocol was modified from Refs. 35 and 36. The sample was kept at 0–4 °C, and buffers contained a protease inhibitor mixture (Roche Applied Science). Five frozen *diutinus* bee abdomens, gut and ovary removed, were homogenized (as in Ref. 31) and centrifuged at 800 × *g* for 10 min in order to exclude exoskeleton and nuclei. The supernatant was centrifuged at 30,000 × *g* for 20 min. The resulting supernatant was filtrated (0.2-μm syringe filter; Pall Corp., Port Washington, NY) and stored as the cytosolic fraction. The membrane-containing pellet was washed three times with 1 ml of HBS, centrifuged at 30,000 × *g* for 20 min, and suspended in HBS containing 0.1% Triton X-100. 24 μg of the cytosolic and the membrane proteins were applied on a 7.5% SDS-polyacrylamide gel and blotted.

Cell Binding Assay—The Sf9 cell test was modified from Ref. 37. Centrifugations were 5 min at 2,000 × *g* in room temperature, and the wash volume was 0.5 ml of PBS, if not specified otherwise. 3.8×10^5 cells in 25 μl of PBS were mixed with 100 μl of filtrated hemolymph diluted 1:10 in PBS, total protein concentration of 1.5 mg/ml, or with 100 μl of fat body protein extract (see Ref. 31), protein concentration 5.7 mg/ml. The negative controls were 25 μl of cells with 100 μl of PBS and 100 μl of hemolymph/fat body protein extract with 25 μl of PBS. The latter ensures that the experiment does not measure possible aggregation of Vg. 0.1 μl of hemolymph and 0.5 μl of fat body extract were kept as untreated controls. The samples were incubated at 28 °C for 50 min with gentle agitation and then washed six times. The final pellet was resuspended in 20 μl of 4 M urea in 10 mM PBS (pH 8), agitated for 15 min, and centrifuged (20 min; 20,800 × *g*). The supernatants were run on a gel and blotted.

FACS—Centrifugation steps were 311 × *g* for 5 min at room temperature, and washing volumes were 200 μl. 0.25 million High Five cells were suspended in 25 μl of PBS (controls) or 0.8 mg/ml fbVg in PBS and incubated for 1 h at 27 °C under agitation. Cells were centrifuged and resuspended in 100 μl of buffer (10 mM HEPES, 140 mM NaCl, and 2.5 mM $CaCl_2$, pH 7.4.). 4 μl of annexin V Alexa Fluor 647 conjugate (Invitrogen) was added, and the samples were incubated for 15 min on ice in the dark. The cells were washed with PBS. 1 μl of 1:10 diluted (in PBS) Fixable Viability Dye eFluor 780 (eBioscience) was added for dead cell detection, and the cells were incubated for 30 min, followed by washing (PBS with 1% BSA (PBS-BSA)). Cells were suspended in 100 μl of PBS-BSA and incubated with the Vg antibody (see "Histology"), 1:2000, for 20 min, followed by three PBS-BSA washes. The samples were incubated with 100 μl of a 1:200 dilution of Alexa-488-conjugated secondary antibody (Sigma) for 20 min, followed by three washes with PBS-BSA. The samples were stored in 100 μl of 2% paraformaldehyde in PBS and analyzed the following day with LSRII (BD Biosciences). To assist the analysis, there was a cells-only sample, a single-color control for each fluorophore, and a Vg-negative sample with secondary antibody for monitoring background staining.

Immunocytochemistry—6.8×10^5 High Five cells were grown on chamber slides (LabTek) overnight. The cells were incubated with 5.3 μM fbVg in PBS (volume 50 μl) purified from honey bee abdomens (see sample purification) for 1 h in 27 °C and washed with HBS. Cells were incubated with 10 μl of annexin V Alexa Fluor 647 conjugate (Invitrogen) in 200 μl of HBS in the dark followed by HBS wash. One sample set was stained for 5 min with 10 μl of propidium iodide (PI) before wash to stain necrotic and late apoptotic cells. Cells were fixed with 2% paraformaldehyde for 10 min and washed twice with ice-cold PBS. 1% BSA in PBS was used for 30-min blocking. The Vg antibody (1:5000) 30-min incubation was followed by three PBS-BSA washes, and the 1:200 Alexa Fluor 488 goat anti-rabbit IgG (Jackson ImmunoResearch) 30-min incubation was followed by three PBS-BSA washes. The fluorescence images were acquired on a Zeiss Axiovert200M fluorescence microscope (Thornwood, NY) using ×20 and ×40 magnification dry objectives, excitation of 492 and 622 nm, and emission of 535 and 668 nm.

We used BSA as a control for nonspecific binding to dead cells. 5×10^5 Sf9 cells killed by freezing (−80 °C) in 50 μl of PBS were incubated with 2.65 μM hlVg or BSA in a total 100-μl volume for 1 h in 27 °C and washed twice with PBS. Fixing, blocking, and antibody treatments were as above, but peptone (Biokar Diagnostics) was used instead of 1% BSA. The anti-BSA primary antibody (produced in rabbits; 1:1000 dilution) was purchased from Invitrogen. The samples were mounted with ProLong Gold reagent with DAPI (Invitrogen). The secondary antibody control was a BSA-treated sample, where primary antibody incubation was omitted. The cells were imaged with a Zeiss Axio Imager M2. All images were processed in ImageJ.

Liposome Preparation—Two kinds of liposomes were prepared: PC and PC + PS in a 1:1 mixture. Egg yolk PC and porcine brain PS (Avanti Polar Lipids, Alabaster, AL) mixed 1:1 with PC were dissolved in chloroform, which was evaporated, resulting in formation of a lipid film. Samples were lyophilized for 2 h to remove traces of chloroform and resuspended in HBS (for surface plasmon resonance (SPR)) or in 10 mM Hepes, 100 mM NaCl, including 12.5 mM 8-aminonaphtalene-1,3,6-trisulfonic acid and 45 mM *p*-xyelene-bis-*N*-pyrimidium bromide, pH 7.0 (for leakage), and left overnight in the dark at room temperature. The hydrated phospholipid solutions were then frozen and thawed seven times, followed by extrusion (11 times) with the Avanti Mini-Extruder using a membrane of 0.1-μm pore size. The leakage-intended liposomes were filtered with a Sephadex G-75 column to remove unencapsulated 8-aminonaphtalene-1,3,6-trisulfonic acid and *p*-xyelene-bis-*N*-pyrimidium bromide. Determination of phospholipid concentration was based on the determination of total phosphorus using a protocol from Avanti Polar Lipids (38). The liposome size was determined by dynamic light scattering (Zetasizer

Nano): PC 102 nm and PS 108 nm for SPR, and PC 122 nm and PS 191 nm for leakage.

SPR—The L1 chip was conditioned with 40 mM octyl glucoside (30 s; flow rate, 30 μl/min) using the Biacore T200 instrument (GE Healthcare). The chip was fully regenerated by injecting 2:3 isopropyl alcohol/NaOH (30 s, 30 μl/min) after each sample injection. Two kinds of liposomes were used: PC and PC + PS in a 1:1 mixture (the latter hereafter referred to as PS). Concentrations of 0.5 mM PC and 1.2 mM PS liposomes were captured on separate channels of the chip (30 s, 10 μl/min), and unbound structures were washed with 10 mM NaOH, followed by a stabilization time of 300 s. The binding temperature was 25 °C, whereas the sample compartment was kept at 4 °C. The liposome surface coverage was verified according to the Biacore user manual's instructions using BSA that binds on the naked chip but has low affinity toward a liposome-covered chip. The following protein concentrations of hlVg, fbVg, the α-helical fragment, and vWFD were used: 0, 100, 500, 1,500, and 2,500 nM. After each sample injection (60 s, flow rate 30 μl/min, dissociation time 600 s), the chip was fully regenerated.

Liposome-combined Proteolysis and LC-MS/MS—PC (size 120 nm) and PS (99 nm) liposomes were incubated with fbVg (see "Liposome Preparation" and "Material Sampling, Protein Purification, and Cell Lines") for 1 h at room temperature in the dark and digested with 25 μg of chymotrypsin for 30 min on ice with the following setup: 1 μl of 0.1 μM liposomes and 8 μl of 0.7 mg/ml fbVg, the total volume adjusted to 12 μl with HBS. The controls were fbVg without liposomes or protease, fbVg with PC or PS, and fbVg with chymotrypsin. The samples were run on a 4–20% SDS-polyacrylamide gel, and band intensities were measured. The protease-resistant band in the liposome samples was excised and analyzed using LC-MS/MS; the gel pieces were washed, treated with 10 mM DTT (Amersham Biosciences) for cysteine reduction, and alkylated using iodoacetamide (Sigma-Aldrich), followed by trypsin digestion. After digestion, the dried samples were dissolved in 11 μl of 0.1% formic acid, and 6 μl was used for injection. The samples were analyzed on a 4000 QTrap (Applied Biosystems/MDS SCIEX, Concord, Canada).

Modeling—A homology model based on lamprey (*Ichthyomyzon unicuspis*) lipovitellin x-ray structure (39, 40) was built using Bodil software (41). The Vgs used for the modeling alignment were as follows: *Bombus ignitus* (Swiss-prot accession number B9VUV6), *Pimpla nipponica* (O17428), *Pteromalus puparum* (B2BD67), *Leucophaea maderae* (Q5TLA5), *Acipenser transmontanus* (Q90243), and *Xenopus laevis* (P18709). Multiple LLTP alignment (42) was also used as a guide. The model was energetically minimized with Discovery Studio (Accelrys, San Diego, CA). PSIPRED was used for secondary structure prediction (43). A segment absent in lamprey Vg was verified to be insect-specific with a multiple alignment against the honey bee amino acid residues Leu^{564}–Leu^{604}. In addition to the species listed above for the modeling alignment, this alignment included Vgs of *Bombus hypocrite* (C7F9J8), *Solenopsis invicta* Vg-2 (Q2VQM6), *Aedes aegypti* (Q16927), *Riptortus clavatus* (O02024), *Anthonomus grandis* (Q05808), *Graptopsaltria nigrofuscata* (Q9U5F1), *Antheraea pernyi* (Q9GUX5), *Periplaneta americana* (Q9U8M0), *Rhyparobia maderae* (Q9GR96), *Blattella germanica* (O76823), *Athalia rosae* (BAA22791), *Encarsia formosa* (AAT48601), *Oreochromis aureus* (Q9YGK0), *Oncorhynchys mykiss* (Q92093), *Fundulus heteroclitus* (Q90508), and human apoB (P04114) and microsomal triglyceride transfer protein (P55157).

Tryptophan Fluorescence—Tryptophan fluorescence of full-length hlVg and the α-helical domain was measured in the presence and absence of PS liposomes at 25 °C on a Cary Eclipse fluorescence spectrophotometer (Agilent Technologies). The measurement was repeated after a 30-min incubation time. The excitation wavelength was set to 295 nm, and the emission spectra were acquired at 310–400 nm using 5-nm slit widths and a scan rate of 600 nm/min. Protein-free blanks were run in parallel with the samples and subtracted from the data.

Extrinsic Fluorescence Measurement—The fluorescence spectra of the leakage assay using the hlVg and fbVg samples were recorded at 25 °C on a Cary Eclipse fluorescence spectrophotometer (Agilent Technologies). Excitation of 8-aminonaphtalene-1,3,6-trisulfonic acid was performed at 355 nm, and its subsequent emission was measured at 510 nm at a scan rate of 600 nm/min. 10- and 20-nm slit widths in the excitation and emission pathways, respectively, were used. A 10-mm quartz cuvette was filled with 1 mM PS liposomes (made of a 1:1 mixture of PC and PS), and 2.5 μM sample was added. The fluorescence was measured every 0.25 min over a time range of 20 min. To estimate the maximum attainable fluorescence, Triton X-100 was added (a final concentration of 2 mM) to ensure disruption of the liposome bilayer at the end of the time scan. The leakage was evaluated as a percentage of complete release of the encapsulated contents with Triton X-100. The initial intensity (at 0 min) of the liposome and sample solution was set to 0% leakage, and the final intensity after adding Triton X-100 corresponded to 100% leakage.

Oxidative Stress Assay—All centrifugation steps were 800 × *g*, 5 min, and 24 °C. 1×10^7 High Five cells were suspended in PBS (control), 5.3 μM BSA, or 5.3 μM fbVg in PBS (volume 50 μl) and incubated for 1 h in 27 °C under gentle agitation. The cells were washed twice with 0.5 ml of PBS. The pellet was suspended in 100 μl of culture medium (Invitrogen). The cells were transferred to 0.4-ml chamber slides (Lab-Tek) that contained 0.3 ml of medium and a final concentration of 1.5 mM H_2O_2. After a 1.5-h incubation, 10 μl of PI in 2× saline-sodium citrate buffer was added for a final concentration of 5 μM. The differences between PI-stained cells of the total cell count in four replicates were analyzed by the χ^2 test. The cells were imaged with a Zeiss Axiovert200M fluorescence microscope using bright field for total cell count and fluorescence filter for dead cell count (excitation 510 nm, emission 630 nm).

RESULTS

Detecting Vg in Honey Bee Tissues and Cell-binding Experiments—We performed immunohistochemistry and Western blot experiments to assess Vg localization in honey bee tissues and to initially test Vg-cell binding. The high resolution confocal micrographs in Fig. 1 represent sections of $n = 5$ individuals for abdominal (Fig. 1, *A–C* and *G–L*) and head tissue samples (Fig. 1, *D–F*). As described previously (29), Vg immunoreactivity (VgIR) is found in the vesicles of fat body trophocytes (Fig. 1, *A–C*). In a subset of these vesicles, we found intense VgIR at the

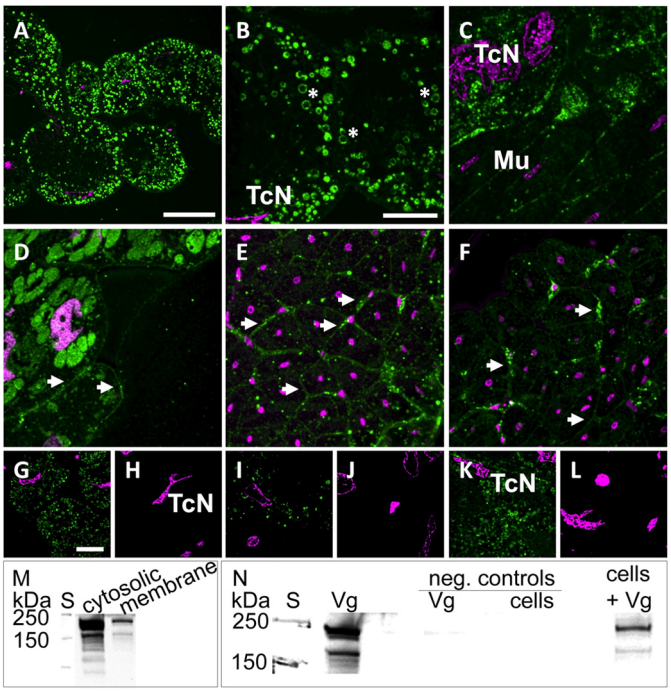

FIGURE 1. **Vg binds to membranes and other cellular structures in the honey bee and to cells of an insect cell line.** *A–L*, immunolabeling indicates the presence of Vg at vesicular (*asterisks*) and cellular membranes (*arrowheads*). Optical sections of abdominal (*A–C*) and head tissue (*D–F*) are labeled with anti-Vg (*green*) and DAPI nuclear stain (*magenta*). *A–C*, trophocytes are identified by irregularly shaped nuclei (*TcN*; see also *G–L*) and contain a large number of Vg-rich vesicles. Intense VgIR was also observed in other abdominal cell types (*e.g.* in muscle tissue (*Mu*)). *D*, hypopharyngeal glands with intense VgIR in Vg-rich granules and less intensely labeled cellular membranes (*arrowheads*). *E* and *F*, syncytial cells of muscle fibers with marked VgIR at their outer membranes (*arrowheads*). *G–L*, test sections treated with anti-Vg (*G*, *I*, and *K*) as compared with alternate negative control sections treated only with the secondary antibody (*H*, *J*, and *L*). The nuclear stain (DAPI) confirms that control and test images were taken from similar sites and cell types (trophocytes with characteristic TcNs). *Scale bars*, 50 μm (*A*), 20 μm (*B–F*), and 20 μm (*G–L*). *M* and *N*, Vg immunoblots detecting full-length Vg (180 kDa) and the 150-kDa Vg fragment present in the abdominal tissue (31). *S*, molecular weight standard. *M*, Vg and its 150-kDa fragment are found in both cytosolic and membrane fractions of abdominal honey bee tissue samples. *N*, Vg of abdominal protein extract binds to Sf9 insect cells during a 1-h incubation (*last lane*, cells + Vg). The *first Vg lane* is a positive control of abdominal protein extract. Negative controls were Vg incubated without cells (*Vg*) and cells without Vg (*cells*).

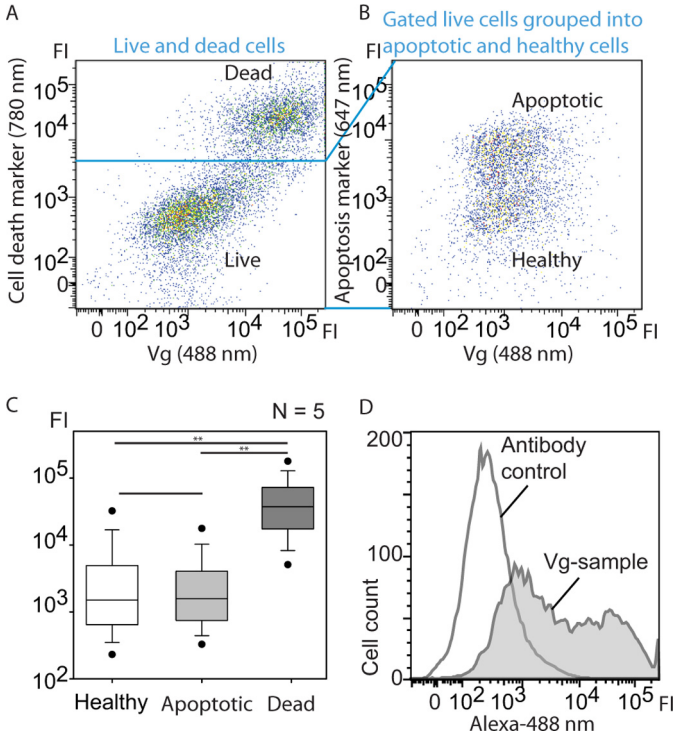

FIGURE 2. **Vg was incubated with High Five insect cells, and the binding was verified by FACS, which revealed high Vg affinity to dead cells.** *A* and *B*, dot plots of Alexa-488-labeled Vg *versus* death cell marker (*A*, Viability Dye®, eBioscience) or apoptosis marker (*B*, annexin V Alexa-647). The emission wavelengths of the fluorescent dyes are indicated. Each *dot* represents a single cell, and the *color gradient* shows the cell density. *FI*, fluorescence intensity. *A*, high vitellogenin signal co-localizes with cell death marker, indicating high affinity with dead cells. *B*, the area in *B* corresponds to an *enlargement* of the live cell plot in *A*. Live cells were separated into early apoptotic (high annexin V fluorescence intensity) and healthy cells that both bind Vg. *C*, statistical presentation of the fluorescence intensities of the $n = 5$ measurements. Vg binding to dead cells is significantly higher than to healthy or early apoptotic cells. *Error bars*, S.E. *D*, Vg-incubated cell sample *versus* background control. Control cells were incubated with the Alexa-488 antibody only.

vesicular membranes (Fig. 1*B*). As expected for an abundant hemolymph protein, VgIR was scattered across different tissue sites (Fig. 1, *C*, *E*, and *F*) apart from the known localization within the cytosol of the cells of the fat body (Fig. 1, *A–C*) and the hypopharyngeal glands (Fig. 1*D*). In particular, intense VgIR was detected at boundary layers (*e.g.* between single cells in hypopharyngeal glands (Fig. 1*D*) or between syncytial cells of muscle fibers (Fig. 1, *E* and *F*)). Our controls for autofluorescence, detector noise, and nonspecific labeling by the secondary antibody were all negative (Fig. 1, *H*, *J*, and *L*; $n = 5$), as compared with test samples recorded with similar microscopy settings (Fig. 1, *G*, *I*, and *K*; $n = 5$). An immunoblot (Fig. 1*M*) shows Vg in both the cytosolic and membrane fraction of abdominal honey bee tissue samples. A 150-kDa Vg fragment that has lost the N-sheet domain (31) is found in both fractions. Finally, Vg binding to standard insect Sf9 cells was positive, including the 150-kDa fragment (Fig. 1*N*). These experiments suggest that honey bee Vg can interact with cells and membranous structures and that this interaction is independent from the putative receptor-binding N-sheet domain that is missing from the 150-kDa Vg fragment.

Vg Binding Is Enhanced to Dead Cells—Next, we explored the idea of an apoB-like anti-inflammatory role of Vg by measuring Vg binding to healthy, apoptotic, and dead cells using cultured insect High Five cells and FACS ($n = 5$). The Vg-incubated cells were separated into dead and live (Fig. 2*A*), and live cells were further separated into apoptotic and healthy cells (Fig. 2*B*). The fluorescence intensity statistics are shown in Fig. 2*C*. The median fluorescence intensities of the healthy, apoptotic, and dead cell populations were found to differ (Kruskal-Wallis analysis of variance: $H = 9.5$, df $= 2$, $p = 0.0087$). Vg binding to dead cells was ~25 times higher than to live cells measured by median fluorescence intensity; this was assessed to be a significant difference by Mann-Whitney *U* post hoc pairwise tests (the values for both healthy and apoptotic cells *versus* dead cells were $Z = 2.6112$, $p = 0.0079$). The binding difference between healthy and apoptotic cells was not significant ($Z = 0.5222$, $p = 0.6905$). The antibody labeling was estimated to be successful because there was low antibody background signal (Fig. 2*D*) and a significant increase in Alexa-488 fluorescence in the Vg-incubated samples ($n = 5$) compared with the antibody control ($n =$

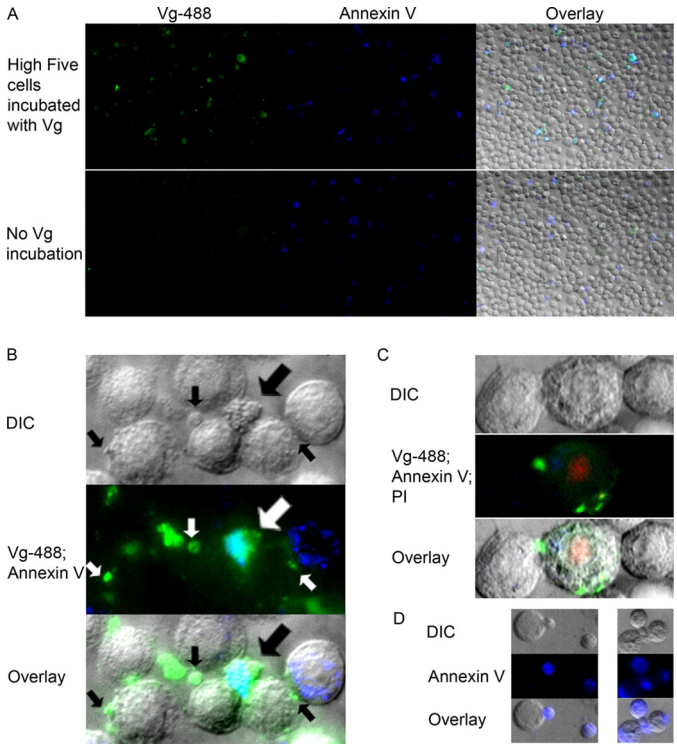

FIGURE 3. **Immunocytochemistry shows Vg affinity to dead cells and cell membrane irregularities.** Vg was labeled with Alexa-488 (*green*), and apoptotic/dead cells were labeled with annexin V Alexa-647 (shown here in *blue*). *A*, the *top row* shows a ×20 magnification of High Five insect cells that were incubated with Vg. Intense Vg signal mostly co-localizes with intense annexin V signal. The *bottom row* is an antibody background control that was not incubated with Vg. Vg and annexin V images are shown separately, and the *last image* is their overlay with a differential interference contrast (*DIC*) image. *B*, ×60 magnification of Vg- and annexin V-bound cells. The *thick arrow* points to the shriveled late apoptotic cell with strong Vg and annexin V co-localization *colored cyan*. Vg also binds heavily to cell membrane irregularities called blebs (*small arrows*). *C*, vitellogenin binds to necrotic cells (the swollen cell in the *middle*). PI (*red*) was used in this sample to mark the nuclei of dead cells. *D*, in the absence of Vg, annexin V binds to cell blebs.

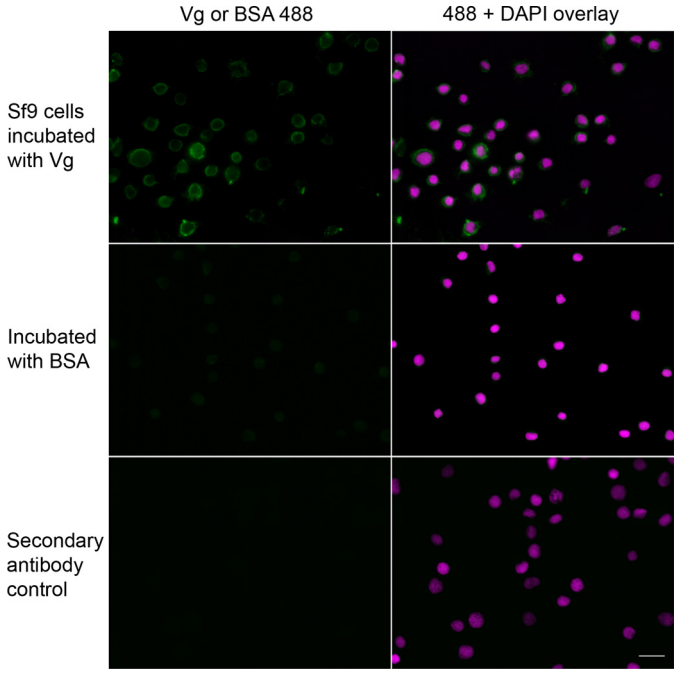

FIGURE 4. **Vg binding to dead Sf9 cells compared with a BSA control.** Killed Sf9 insect cells were incubated with Vg or BSA, followed by a treatment using rabbit anti-Vg or rabbit anti-BSA polyclonal primary antibody. The secondary antibody control was not incubated with a primary antibody, and, as expected, marked fluorescence was absent in these samples. All samples were treated with Alexa-488 (*green*) secondary antibody and DAPI. In contrast to Vg-incubated cells, the controls incubated with BSA did not exhibit marked positive staining, suggesting that binding of BSA was negligible. *Scale bar*, 20 μm.

3) (Mann-Whitney *U* test; $Z = 2.2361$, $p = 0.03571$). In brief, all cell populations bound Vg, but the binding was significantly higher in the case of dead cells.

To obtain detailed information about the Vg localization on a damaged cell surface, we performed fluorescence imaging using High Five and Sf9 cells that were incubated with Vg. The antibody background was low (Fig. 3*A* (*No Vg incubation*) and the *bottom panel* in Fig. 4 (no primary antibody (*Secondary antibody control*)). We observed strong Vg localization on the late apoptotic cells (Fig. 3*B*) that were identified by their morphology (small, irregular) and by their strong binding of our positive control protein, annexin V. Furthermore, we found Vg bound to cell blebs that are signs of a damaged cell (Fig. 3*B*). Also, Vg bound to necrotic cells (Fig. 3*C*) that were identified by morphology (large, rough surface) and PI staining. In the absence of Vg, the apoptosis marker annexin V, which binds to PS, bound to cell blebs (Fig. 3*D*), but this binding appears to be inhibited in the presence of Vg (Fig. 3*B*). Thus, some of the annexin V-negative cells, determined to be healthy in the FACS experiment, might be damaged and blebby. In Fig. 4, another serum protein, BSA, was used as a negative control for dead cell binding. BSA was binding very weakly compared with the markedly positive Vg signal on the dead cells' surface.

SPR Measurement of Lipid Bilayer Binding—Because Vg shows differentiated cell surface binding, a question opens as to what mediates the binding. To test whether the phospholipid bilayer in itself can contribute to the affinity, we tested honey bee Vg binding to PC and PS/PC 1:1 mixture liposomes (the mixture is hence called PS) using an SPR technique. PC is a major lipid on insect cell membranes (44). Because Vg appears to selectively bind more strongly to dead cells and the PS-rich cell blebs (see above) compared with healthy cells, PS-liposomes were used as a simple model of damaged or dead cell membrane.

We used two types of native samples purified from a large set of honey bees: full-length Vg purified from hemolymph (hlVg) and predominantly fragmented Vg (the previously described 150-kDa fragment) purified from fat body (fbVg). In addition, two domains were produced in *Escherichia coli*: the α-helical and vWFD domain, which both localize to the 150-kDa fragment of Vg. The vWFD domain produced in *E. coli* did not bind to the liposomes (Fig. 5), but the sensograms of all the other samples indicate that the Vg molecules become permanently associated with the bilayers (Fig. 5*A*). In every case, the binding response to PS exceeded that of PC. The full-length hlVg had the highest affinity to both bilayers. The predominantly 150-kDa fbVg fragment had slightly lower affinity than the full-length hlVg. The α-helical domain alone, moreover, showed a similar response to fbVg (Fig. 5, *A* and *B*), particularly when bound to PS. $S_{0.5}$ is the protein concentration that yields half of the maximal response. This binding affinity value was calculated for hlVg based on the affinity curve of the five measure-

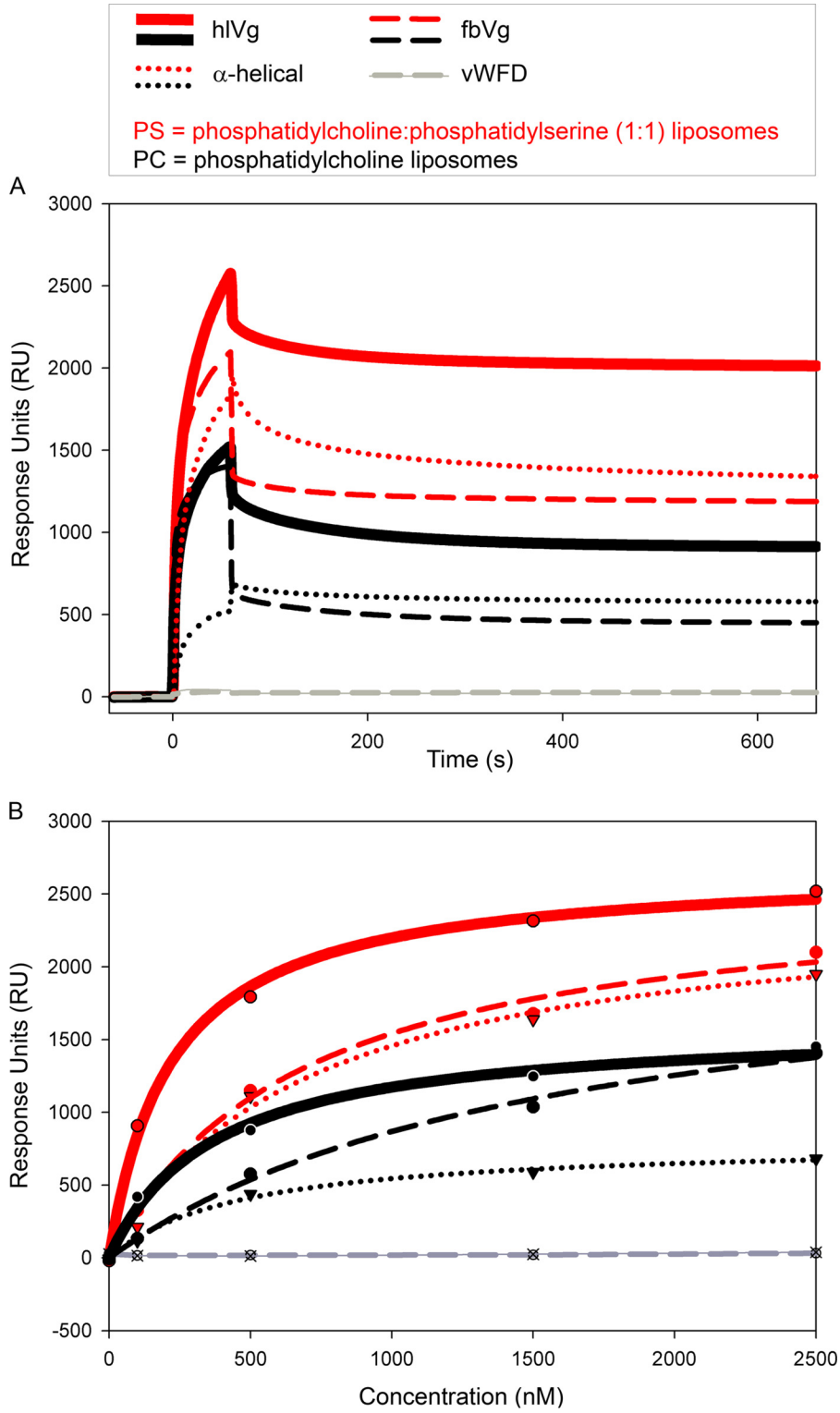

FIGURE 5. **SPR measurements of Vg binding to PS and PC bilayers.** *Red*, PS; *black*, PC. *Thick lines*, hlVg; *dashed lines*, fbVg; *dotted lines*, α-helical fusion domain Vg. The vWFD domain is illustrated in *gray*. *A*, all sensograms of the 2,500 nM samples except from the vWFD domain show irreversible binding to the bilayers; none of the samples that bound returned back to the base line during the dissociation time (600 s). *B*, response units (*RU*) as a function of concentration. These *curves* were fitted based on R_{max} values of the measurements done at sample concentrations of 0, 100, 500, 1,500, and 2,500 nM, marked with *dots*, *triangles*, or *crosses*. The fastest association is seen with full-length Vg on PS (the *steepest red curve*; hlVg). The α-helical recombinant domain binding pattern on PS is nearly identical to the binding pattern of the native fbVg (the *red curves* in *dotted* and *dashed lines*, respectively).

ments (Fig. 5*B*). hlVg $S_{0.5}$ with PC was 367 ± 80, and with PS it was 219 ± 26. The given S.E. is based on the curve fitting.

Limited Proteolysis of Vg in the Presence of Liposomes—In addition to SPR, another approach was used to verify Vg-liposome interaction: limited proteolysis in combination with liposomes. This method also provides a rough insight into the protein region that interacts with the bilayers, because this region can become protected against proteolysis. fbVg, incubated with

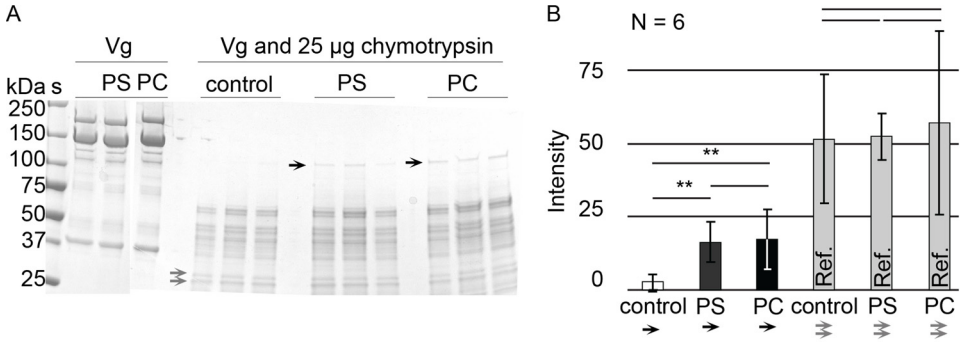

C

```
   1 MLLLLTLLLF AGTVAADFQH NWQVGNEYTY LVRSRTLTSL GDLSDVHTGI
  51 LIKALLTVQA KDSNVLAAKV WNGQYARVQQ SMPDGWETEI SDQMLELRDL
 101 PISGKPFQIR MKHGLIRDLI VDRDVPTWEV NILKSIVGQL QVDTQGENAV
 151 KVNSVQVPTD DEPYASFKAM EDSVGGKCEV LYDIAPLSDF VIHRSPELVP
 201 MPTLKGDGRH MEVIKIKNFD NCDQRINYHF GMTDNSRLEP GTNKNGKFFS
 251 RSSTSRIVIS ESLKHFTIQS SVTTSKMMVS PRLYDRQNGL VLSRMNLTLA
 301 KMEKTSKPLP MVDNPESTGN LVYIYNNPFS DVEERRVSKT AMNSNQIVSD
 351 NSLSSSEEKL KQDILNLRTD ISSSSSSISS SEENDFWQPK PTLEDAPQNS
 401 LLPNFVGYKG KHIGKSGKVD VINAAKELIF QIANELEDAS NIPVHATLEK
 451 FMILCNLMRT MNRKQISELE SNMQISPNEL KPNDKSQVIK QNTWTVFRDA
 501 ITQTGTGPAF LTIKEWIERG TTKSMEAANI MSKLPKTVRT PTDSYIRSFF
 551 ELLQNPKVSN EQFLNTAATL SFCEMIHNAQ VNKRSIHNNY PVHTFGRLTS
 601 KHDNSLYDEY IPFLERELRK AHQEKDSPRI QTYIMALGMI GEPKILSVFE
 651 PYLEGKQQMT VFQRTLMVGS LGKLTETNPK LARSVLYKIY LNTMESHEVR
 701 CTAVFLLMKT NPPLSMLQRM AEFTKLDTNR QVNSAVKSTI QSLMKLKSPE
 751 WKDLAKKARS VNHLLTHHEY DYELSRGYID EKILENQNII THMILNYVGS
 801 EDSVIPRILY LTWYSSNGDI KVPSTKVLAM ISSVKSFMEL SLRSVKDRET
 851 IISAAEKIAE ELKIVPEELV PLEGNLMINN KYALKFFPFD KHILDKLPTL
 901 ISNYIEAVKE GKFMNVNMLD TYESVHSFPT ETGLPFVYTF NVIKLTKTSG
 951 TVQAQINPDF AFIVNSNLRL TFSKNVQGRV GFVTPFEHRH FISGIDSNLH
1001 VYAPLKISLD VNTPKGNMQW KIWPMKGEEK SRLFHYSVVP FVSNHDILNL
1051 RPLSMEKGTR PMIPDDNTSL ALPKNEGPFR LNVETAKTNE EMWELIDTEK
1101 LTDRLPYPWT MDNERYVKVD MYMNLEGEQK DPVIFSTSFD SKVMTRPDTD
1151 SENWTPKMMA VEPTDKQANS KTRRQEMMRE AGRGIESAKS YVVDVRVHVP
1201 GESESETVLT LAWSESNVES KGRLLGFWRV EMPRSNADYE VCIGSQIMVS
1251 PETLLSYDEK MDQKPKMDFN VDIRYGKNCG KGERIDMNGK LRQSPRLKEL
1301 VGATSIIKDC VEDMKRGNKI LRTCQKAVVL SMLLDEVDIS MEVPSDALIA
1351 LYSQGLFSLS EIDNLDVSLD VSNPKNAGKK KIDVRAKLNE YLDKADVIVN
1401 TPIMDAHFKD VKLSDFGFST EDILDTADED LLINNVFYED ETSCMLDKTR
1451 AQTFDGKDYP LRLGPCWHAV MTTYPRINPD NHNEKLHIPK DKSVSVLSRE
1501 NEAGQKEVKV LLGSDKIKFV PGTTSQPEVF VNGEKIVVSR NKAYQKVEEN
1551 EIIFEIYKMG DRFIGLTSDK FDVSLALDGE RVMLKASEDY RYSVRGLCGN
1601 FDHDSTNDFV GPKNCLFRKP EHFVASYALI SNQCEGDSLN VAKSLQDHDC
1651 IRQERTQQRN VISDSESGRL DTEMSTWGYH HNVNKHCTIH RTQVKETDDK
1701 ICFTMRPVVS CASGCTAVET KSKPYKFHCM EKNEAAMKLK KRIEKGANPD
1751 LSQKPVSTTE ELTVPFVCKA
```

FIGURE 6. **A ~120-kDa Vg segment is resistant to proteolysis in the presence of liposomes.** *A*, a gel showing how a part of Vg (the band marked with *black arrows*) is not digested by chymotrypsin in the presence of PC or PS liposomes. The *gray arrows* show two bands, whose intensity in all *lanes* was used as a reference. *S*, molecular weight standard. *Vg*, untreated, purified Vg from honey bee abdomen. *Control*, no liposomes. *PS*, Vg with PS liposomes. *PC*, Vg with PC liposomes. *B*, the intensity of the bands marked with *black arrows* in *A* is significantly higher than the intensity of the corresponding gel region in the controls but does not differ between PS and PC. The reference bands (*gray columns*; *gray arrows* in *A*) showed no significant difference. The *error bars* show the S.D. of six band intensities. *C*, the LC-MS/MS hits (*red*) of the gel-extracted honey bee Vg segment that resists chymotrypsin digestion in the presence of liposomes (*black arrows* in *A*). The α-helical domain is *highlighted gray*. The most reliable peptide hits with high Mascot ion score (>75) are *underlined*.

PC or PS, was enzymatically digested and run on gel (Fig. 6*A*). In the presence of liposomes, a ~120-kDa putatively membrane-embedded part of Vg was less degradable. LC-MS/MS hits of this segment span amino acid residues 135–1613 (Fig. 6*C*). This region contains the α-helical domain (residues 416–765). In order to quantify the gel experiment and to see if there is any difference between Vg bands in the PC and PS samples, the intensities of the protease-resistant gel bands were measured ($n = 6$). PC and PS sample band intensities differed from the corresponding, nearly zero, background gel region in the liposome-free control (Kruskal-Wallis analysis of variance; $H = 10.75$, $p = 0.005$; Fig. 6*B*) but not from each other (Mann-Whitney post hoc test; $Z = 0.16$, $p = 0.873$; Fig. 6*A*). For reference, we measured a gel region in the range of ~25 kDa (Fig. 6*A*), where no intensity differences were found (Kruskal-Wallis analysis of variance; $H = 0.047$, $p = 0.977$; Fig. 6*B*), indicating

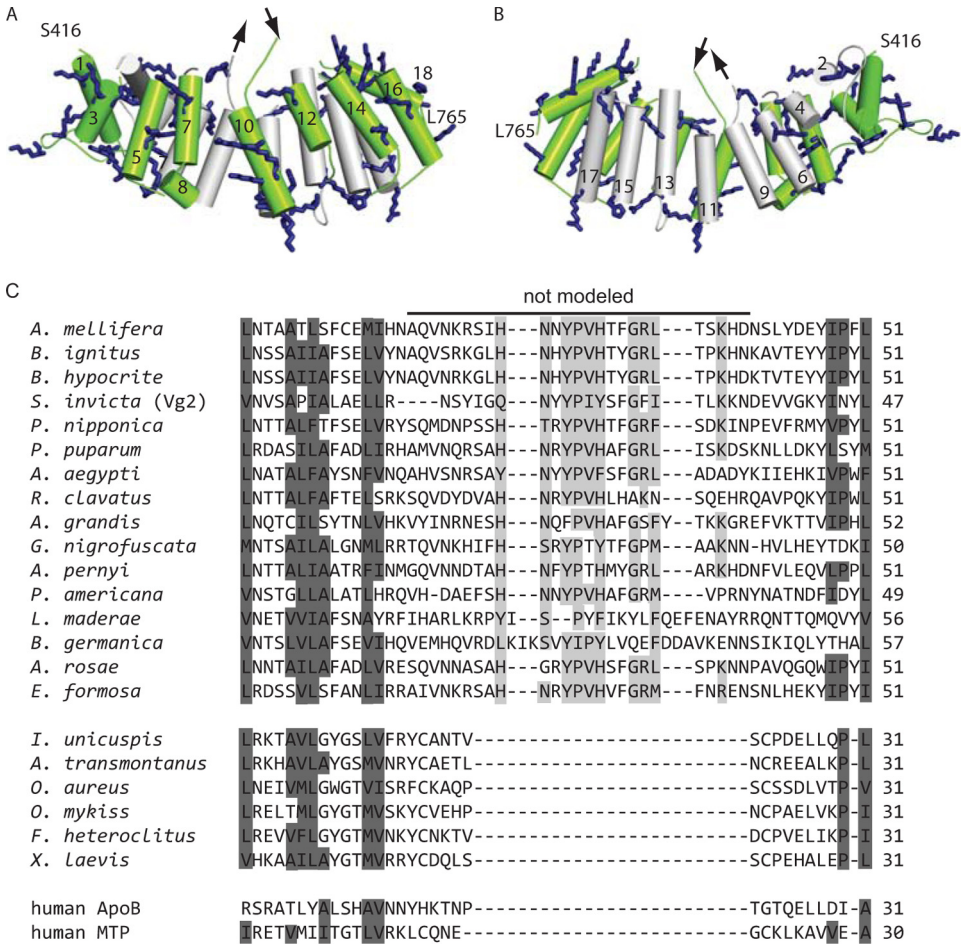

FIGURE 7. **A homology model of the 18-helix α-helical domain of honey bee Vg.** The positively charged residues are shown as *blue sticks*. The 25-residue region that could not be modeled is marked with *arrows*. The model begins at serine 416 and ends at leucine 765. *A*, the helices facing the solvent (*green*) carry 34 solvent-facing positively charged residues that might participate in lipid interactions. *B*, the helices facing the lipid-binding cavity (*gray*). *C*, a multiple alignment of the segment that is absent in the structure template (*Ichthyomyzon unicuspis* lipovitellin). This predicted loop is conserved in the 16 insect species included in the alignment; however, the five fish, an amphibian (*Xenopus laevis*), and the human homologues lack this prolonged loop. Highly conserved LLTP residues are *highlighted dark gray*. Many of the loop residues are conserved in insects (*light gray*).

that the digestion is generally similar in the control and the liposome samples with the exception of the ~120 kDa band. This experiment adds to the SPR data, indicating that a part of Vg is able to integrate into both PC and PS liposomes, and this part contains the α-helical subdomain.

Homology Modeling—Because the α-helical part of Vg appears to be able to interact with lipid bilayers, we modeled it in order to better understand the structural basis of this interaction. Our homology model shows a total of 49 positively charged residues, 34 of which point directly to the solvent (Fig. 7*A*). The side facing the binding cavity of Vg is less charged, as expected because Vg carries hydrophobic molecules in this cavity (Fig. 7*B*). The secondary structure prediction program PSIPRED (43) assigned the domain exclusively to helices with connective loops that support the accuracy of the helix locations in the model (data not shown). Residues 579–603 could not be modeled because they are absent in the template (lamprey lipovitellin); PSIPRED prediction suggests that this missing sequence is a random coil (data not shown). Based on our alignment of Vgs of insects and vertebrates and the related human proteins, we assign the loop as insect-specific (Fig. 7*C*). Some of the amino acid residues in the loop are well conserved in insects: His^{587}, Tyr^{590}, Pro^{591}, Val^{592}, His^{593}, Gly^{596}, Arg^{597}, Leu^{598}, and Lys^{601} (*highlighted light gray* in Fig. 6*C*).

Tryptophan Fluorescence—For detection of possible conformational changes upon liposome binding, we measured tryptophan fluorescence of full-length Vg and the α-helical domain. Vg (without its signal peptide) contains 17 tryptophan residues at various locations in the sequence, three of which are located in the α-helical domain (Fig. 8). If the chemical environment of these sites underwent major structural changes, a shift in the protein's tryptophan fluorescence spectrum would be expected. However, no shift was observed for either of the samples (Fig. 8). The fluorescence intensity was quenched in the liposome-bound samples compared with the liposome-free samples, as expected.

The Effect of Vg Binding Measured by Fluorescence Leakage and Oxidative Stress Tests—After the demonstrations of Vg-cell and Vg-bilayer binding, we tested two possible biological functions of the binding to bilayers/cells. First, Vg binding to PS-enriched dying cells might cause disruptive membrane rearrangements that facilitate cytolysis (45). Therefore, we tested the effect of hemolymph and fat body purified native Vg on the integrity of PS liposomes. We used an extrinsic fluorescence

leakage assay, which monitors the release of a fluorophore and its quencher encapsulated in vesicles. The fluorescence signal was not notably changed until the final 2.5 μM protein concentration (the same as used in SPR); thus, Vg-mediated disruptive membrane activity found no support in the experiment (Fig. 9*A*). Second, Vg binding to healthy cells could be connected to the antioxidant properties of Vg. In our ROS test, Vg-incubated insect cells (High Five) were found to be more tolerant against H_2O_2-induced oxidative stress than any of our two controls (Fig. 9, *B* and *C*). The controls were cells incubated with buffer and cells incubated with BSA. An overall χ^2 test between the Vg-treated samples and the double controls was significant ($\chi^2 = 54.0932$, df = 2, $p = 1.794e{-}12$). Vg enhanced the survival of the cells significantly compared with the buffer control ($\chi^2 = 33.6257$, df = 1, $p = 6.68e{-}09$) and the BSA control ($\chi^2 = 46.3796$, df = 1, $p = 9.743e{-}12$). The two controls did not differ ($\chi^2 = 0.7335$, df = 1, p value = 0.3918).

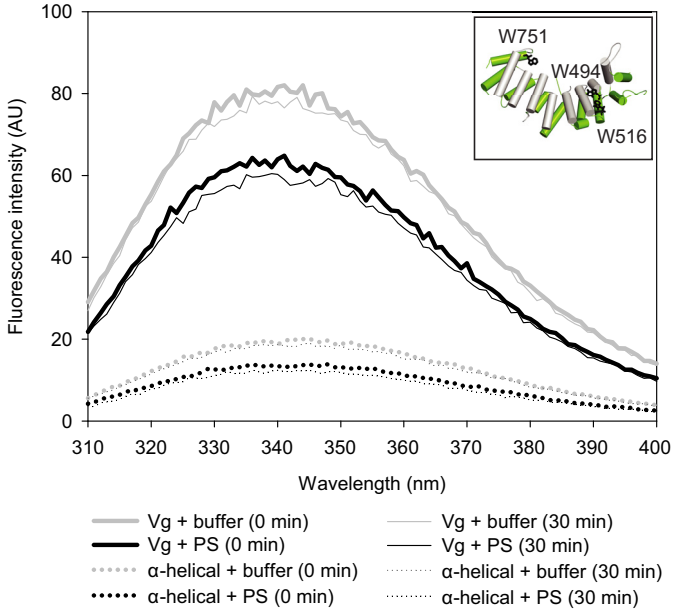

FIGURE 8. **Tryptophan fluorescence of vitellogenin (*solid line*) and its α-helical domain (*dotted line*) upon liposome binding.** The three tryptophan residues of the α-helical domain are indicated as *black sticks* in the model (*inset*). The fluorescence intensity of the protein samples was measured at time 0 (*thick lines*) and after 30 min (*thin lines*). Samples with no liposomes are shown in *gray*, and the samples with PS liposomes are shown in *black*. Liposomes appear to quench the tryptophan signal, but no shifts in the tryptophan emission peaks were observed. Protein-free blanks were measured in parallel with the samples, and the curves are blank-subtracted. The curves represent the average of three parallel measurements.

DISCUSSION

Many serum proteins, including LLTPs, have affinity to exposed hydrophobic molecules and surfaces that often signal danger. This work shows for the first time that honey bee Vg has similar properties. Immunohistochemistry of honey bee tissues and Western blotting show that Vg is associated with cells and membranous structures in healthy tissues. Further FACS and imaging experiments detailed that Vg affinity with dead cells and membrane blebs is enhanced. We suggest that direct Vg binding to cell membrane phospholipids is involved because SPR and limited proteolysis in combination with liposomes support Vg-bilayer binding. The binding can be linked to the antioxidative and putative anti-inflammatory defense mechanisms of Vg in the honey bee.

Vgs have reproductive (egg yolk precursor) and non-reproductive (behavior, immunity) roles. The N-sheet domain is the predicted receptor binding site of Vgs and presumably essential for the uptake of the protein by oocytes (19). In honey bees, the N-sheet is under strong negative selection (*i.e.* mutational change is not permitted) (46), yet our observations (Figs. 1 (*M* and *N*), 5, and 6) suggest that Vg is able to adhere to lipid bilayers without receptor interaction. In the current literature, only one study documents a Vg-membrane association, and this interaction was shown for reproductive cells. In the amphibian

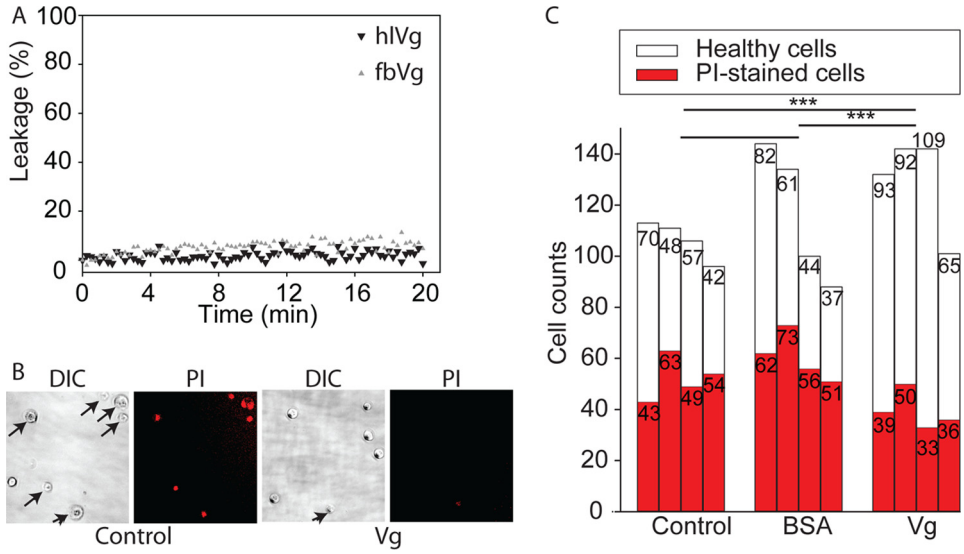

FIGURE 9. **Indications of a non-disruptive Vg-bilayer binding and protection of cells against oxidative stress.** *A*, content release from PS liposomes in response to hlVg or fbVg at a concentration of 2.5 μM. The fluorescence signal at 0 min was set to 0%, and 100% leakage corresponds to the signal of liposomes fully disrupted by Triton X-100. Vg samples do not cause notable leakage, which means that the integrity of PS liposomes is not affected by Vg. *B*, insect cells were coated with purified Vg, carefully washed, and subjected to 1.5 mM H_2O_2 for 1.5 h. Total cells were counted using differential interference contrast (*DIC*) microscopy, and PI staining was used as a cell death indicator. *C*, counts of healthy (*white*) and PI-stained (*red*) cells of $n = 4$ experiments, where cells were incubated with either buffer, BSA, or Vg. Vg-coated cells showed significant reduction in PI staining compared with the controls.

Discoglossus pictus, lipovitellin (*i.e.* cleaved Vg in eggs) appears at the surface of each egg at a particular sperm binding site, where lipovitellin is involved in sperm-egg interaction (47). Our data of Vg on somatic cells, including muscle cells, of functionally sterile honey bee workers suggests that Vg-cell interaction can be non-reproductive. The 150-kDa Vg fragment (Vg without the N-sheet) has been (and still is) under considerable positive selection, not only in honey bees but in several *Apis* species (46). The reasons for the positive selection of the Vg sequence subsequent to the N-sheet have been purely speculative (46, 48), but we suggest that membrane affinity could be involved in this evolution.

Honey bee Vg binding to dead and damaged (blebbing) cells suggests that Vg can be an anti-inflammatory actor similar to many other plasma proteins (6). The mechanism of dead cell recognition can be explained, to some extent, by the enhanced affinity of Vg for the PS bilayer in the SPR measurements. The affinity difference was not revealed by SDS-PAGE (Fig. 6), which might be due to the known shortcomings of SDS-PAGE, in particular the poorer resolution of signal differences in quantitative analysis. PS is exposed on the membrane of apoptotic and dead cells. PS is found concentrated on blebs (49), where our imaging data show high Vg occupation and inhibition of the binding of our positive control, annexin V. Similar annexin V inhibition is recorded for other bleb-binding serum proteins (50). However, Vg does not appear to make a difference between healthy and early apoptotic cells, the latter being clearly stained by annexin V. Annexin V-PS affinity is affected by PS percentage, phospholipid clustering and immobilization, calcium strength, membrane curvature and rigidity, and protein clustering on the membrane (51). Vg might be sensitive to such factors, and perhaps the protein does not favor the conditions on the membrane of early apoptotic cells. Because LLTPs are broad spectrum pattern recognition receptors, it is possible that Vg binds to additional molecules that are exposed on dead cells or blebs, such as DNA, proteins, or glycans. However, further studies are needed to verify the binding mechanism and to reveal the downstream effects of Vg-damaged cell recognition. Our leakage assay results indicate that Vg binding on PS-rich bilayer does not damage the membrane. Potentially, Vg binding could promote the clearance of damaged cells, as is seen in several plasma proteins (9, 52–54).

The Vg domain (the N-sheet in combination with the α-helical subdomain) association with lipid surfaces has been described previously in human apoB (15, 17). We narrow down this property to the α-helical part in the honey bee. The positively charged solvent-facing side of the α-helix is probably attracted by the negative charge of especially the PS of blebbing or otherwise compromised cellular membranes. For example, arginine residues are important for PS binding of annexin V (55). Our fluorescence data do not suggest major structural rearrangements upon liposome binding for the full-length Vg or the α-helical domain. A likely explanation is that the binding is mediated by the loops between the helices or by some of the 15 helices with no tryptophan. Both Vg and the domain show typical changes in tryptophan fluorescence emission intensity when measured bound to liposomes.

Because the phospholipid affinity of Vg domain is now reported for as phylogenetically distant proteins as human apoB and honey bee Vg, it is tempting to interpolate this property to other LLTPs. However, the relatively well conserved Vg domain has great variation among species at two sites. One is the linker between the N-sheet and the α-helix. This linker is elongated and heavily phosphorylated in most insects compared with vertebrate Vgs (32), and its length and the number of phosphorylation sites varies tremendously within insects (3). The other variable site was identified in this study; there is a loop in the middle of the α-helical that is well conserved in insects but absent in higher animals. These structural differences within the Vg domain can have an effect on affinity or binding selectivity of LLTPs.

Vg binding to healthy cells is visible in our histology and FACS data and is supported by Vg binding to PC liposomes. In the images of cultured cells (Fig. 3), however, Vg binding to healthy cells was hardly visible and was largely overshadowed by the bright signal of the blebs and dead cells. Even if Vg binds only weakly to cultured cells, we show that Vg shields these cells against H_2O_2 damage. Previous studies have shown that honey bees with a higher Vg titer in hemolymph are more resistant to oxidative stress, and Vg is the major target of oxidative carbonylation (23). Our results strengthen this view. The membrane might be the optimal location for Vg to provide direct shielding for the cell against a ROS attack because lipids are chemically prone to oxidation (56).

Chronic inflammatory responses are connected to severe health conditions prevalent in the Western world (cardiovascular diseases, diabetes, Alzheimer disease, obesity, and cancer (57, 58)), and in all these, apoB is involved. This makes LLTPs exceedingly interesting proteins for medical research. The long lived wintertime honey bee workers accumulate Vg in hemolymph and fat tissue, and Vg is thought to play a central role in the extended life span of the winter bees (23, 28, 29, 59–62). We show how Vg not only helps cells to battle ROS but might also inform the body about tissue damage. Vgs, although extensively studied, in particular in fish (20), have not traditionally been viewed from the inflammatory perspective. Our study highlights that the honey bee offers a simple model system for understanding the complicated physiological effects of LLTPs.

Acknowledgments—We thank Prof. Martinez and Sundström for access to instruments and reagents. We especially thank Martinez for expert advice. We also thank Knut Teigen for the model minimization and Ole Horvli, Duane Moogk, and Karolina Malecek for kind assistance with the methods. We thank the following beekeeper experts for the honey bee samples: Claus Kreibich (Norwegian University of Life Sciences), Andrew Coté (New York City Beekeepers Association), James Johnson (Narrows Botanical Garden), and Robert Deschak.

REFERENCES

1. Hayward, A., Takahashi, T., Bendena, W. G., Tobe, S. S., and Hui, J. H. (2010) Comparative genomic and phylogenetic analysis of vitellogenin and other large lipid transfer proteins in metazoans. *FEBS Lett.* **584,** 1273–1278
2. Baker, M. E. (1988) Is vitellogenin an ancestor of apolipoprotein B-100 of human low-density lipoprotein and human lipoprotein lipase? *Biochem. J.*

255, 1057–1060
3. Tufail, M., and Takeda, M. (2008) Molecular characteristics of insect vitellogenins. *J. Insect. Physiol.* **54,** 1447–1458
4. Tseng, D. Y., Chen, Y. N., Kou, G. H., Lo, C. F., and Kuo, C. M. (2001) Hepatopancreas is the extraovarian site of vitellogenin synthesis in black tiger shrimp, *Penaeus monodon*. *Comp. Biochem. Physiol. A Mol. Integr. Physiol.* **129,** 909–917
5. Litvack, M. L., and Palaniyar, N. (2010) Review. Soluble innate immune pattern-recognition proteins for clearing dying cells and cellular components. Implications on exacerbating or resolving inflammation. *Innate Immun.* **16,** 191–200
6. Seong, S. Y., and Matzinger, P. (2004) Hydrophobicity. An ancient damage-associated molecular pattern that initiates innate immune responses. *Nat. Rev. Immunol.* **4,** 469–478
7. Kemper, C., Atkinson, J. P., and Hourcade, D. E. (2010) Properdin. Emerging roles of a pattern-recognition molecule. *Annu. Rev. Immunol.* **28,** 131–155
8. Korb, L. C., and Ahearn, J. M. (1997) C1q binds directly and specifically to surface blebs of apoptotic human keratinocytes. Complement deficiency and systemic lupus erythematosus revisited. *J. Immunol.* **158,** 4525–4528
9. Ogden, C. A., deCathelineau, A., Hoffmann, P. R., Bratton, D., Ghebrehiwet, B., Fadok, V. A., and Henson, P. M. (2001) C1q and mannose binding lectin engagement of cell surface calreticulin and CD91 initiates macropinocytosis and uptake of apoptotic cells. *J. Exp. Med.* **194,** 781–795
10. Wang, S., Wang, Y., Ma, J., Ding, Y., and Zhang, S. (2011) Phosvitin plays a critical role in the immunity of zebrafish embryos via acting as a pattern recognition receptor and an antimicrobial effector. *J. Biol. Chem.* **286,** 22653–22664
11. Zhang, S., Wang, S., Li, H., and Li, L. (2011) Vitellogenin, a multivalent sensor and an antimicrobial effector. *Int. J. Biochem. Cell Biol.* **43,** 303–305
12. Vreugdenhil, A. C., Snoek, A. M., van 't Veer, C., Greve, J. W., and Buurman, W. A. (2001) LPS-binding protein circulates in association with apoB-containing lipoproteins and enhances endotoxin-LDL/VLDL interaction. *J. Clin. Invest.* **107,** 225–234
13. Berger, D., Schleich, S., Seidelmann, M., and Beger, H. G. (1990) Correlation between endotoxin-neutralizing capacity of human plasma as tested by the limulus-amebocyte-lysate-test and plasma protein levels. *FEBS Lett.* **277,** 33–36
14. Cho, N. H., and Seong, S. Y. (2009) Apolipoproteins inhibit the innate immunity activated by necrotic cells or bacterial endotoxin. *Immunology* **128,** e479–486
15. Ledford, A. S., Weinberg, R. B., Cook, V. R., Hantgan, R. R., and Shelness, G. S. (2006) Self-association and lipid binding properties of the lipoprotein initiating domain of apolipoprotein B. *J. Biol. Chem.* **281,** 8871–8876
16. Richardson, P. E., Manchekar, M., Dashti, N., Jones, M. K., Beigneux, A., Young, S. G., Harvey, S. C., and Segrest, J. P. (2005) Assembly of lipoprotein particles containing apolipoprotein-B. Structural model for the nascent lipoprotein particle. *Biophys. J.* **88,** 2789–2800
17. Ledford, A. S., Cook, V. A., Shelness, G. S., and Weinberg, R. B. (2009) Structural and dynamic interfacial properties of the lipoprotein initiating domain of apolipoprotein B. *J. Lipid Res.* **50,** 108–115
18. Sivaram, P., Choi, S. Y., Curtiss, L. K., and Goldberg, I. J. (1994) An amino-terminal fragment of apolipoprotein B binds to lipoprotein lipase and may facilitate its binding to endothelial cells. *J. Biol. Chem.* **269,** 9409–9412
19. Li, A., Sadasivam, M., and Ding, J. L. (2003) Receptor-ligand interaction between vitellogenin receptor (VtgR) and vitellogenin (Vtg), implications on low density lipoprotein receptor and apolipoprotein B/E. The first three ligand-binding repeats of VtgR interact with the amino-terminal region of Vtg. *J. Biol. Chem.* **278,** 2799–2806
20. Finn, R. N. (2007) Vertebrate yolk complexes and the functional implications of phosvitins and other subdomains in vitellogenins. *Biol. Reprod.* **76,** 926–935
21. Tsimikas, S., and Miller, Y. I. (2011) Oxidative modification of lipoproteins. Mechanisms, role in inflammation and potential clinical applications in cardiovascular disease. *Curr. Pharm. Des.* **17,** 27–37
22. Tomkin, G. H. (2010) Atherosclerosis, diabetes and lipoproteins. *Expert Rev. Cardiovasc. Ther.* **8,** 1015–1029
23. Seehuus, S. C., Norberg, K., Gimsa, U., Krekling, T., and Amdam, G. V. (2006) Reproductive protein protects functionally sterile honey bee workers from oxidative stress. *Proc. Natl. Acad. Sci. U.S.A.* **103,** 962–967
24. Harman, D. (1956) Aging. A theory based on free radical and radiation chemistry. *J. Gerontol.* **11,** 298–300
25. Villalba, J. M., Navarro, F., Gómez-Díaz, C., Arroyo, A., Bello, R. I., and Navas, P. (1997) Role of cytochrome b_5 reductase on the antioxidant function of coenzyme Q in the plasma membrane. *Mol. Aspects Med.* **18,** S7–S13
26. Cha, M. K., Yun, C. H., and Kim, I. H. (2000) Interaction of human thiol-specific antioxidant protein 1 with erythrocyte plasma membrane. *Biochemistry* **39,** 6944–6950
27. Amdam, G. V., Simões, Z. L., Hagen, A., Norberg, K., Schrøder, K., Mikkelsen, Ø., Kirkwood, T. B., and Omholt, S. W. (2004) Hormonal control of the yolk precursor vitellogenin regulates immune function and longevity in honeybees. *Exp. Gerontol.* **39,** 767–773
28. Amdam, G. V., Aase, A. L., Seehuus, S. C., Kim Fondrk, M., Norberg, K., and Hartfelder, K. (2005) Social reversal of immunosenescence in honey bee workers. *Exp. Gerontol.* **40,** 939–947
29. Smedal, B., Brynem, M., Kreibich, C. D., and Amdam, G. V. (2009) Brood pheromone suppresses physiology of extreme longevity in honeybees (*Apis mellifera*). *J. Exp. Biol.* **212,** 3795–3801
30. Dainat, B., Evans, J. D., Chen, Y. P., Gauthier, L., and Neumann, P. (2012) Predictive markers of honey bee colony collapse. *PLoS One* **7,** e32151
31. Havukainen, H., Halskau, Ø., Skjaerven, L., Smedal, B., and Amdam, G. V. (2011) Deconstructing honeybee vitellogenin. Novel 40 kDa fragment assigned to its N terminus. *J. Exp. Biol.* **214,** 582–592
32. Havukainen, H., Underhaug, J., Wolschin, F., Amdam, G., and Halskau, Ø. (2012) A vitellogenin polyserine cleavage site. Highly disordered conformation protected from proteolysis by phosphorylation. *J. Exp. Biol.* **215,** 1837–1846
33. Seehuus, S. C., Norberg, K., Krekling, T., Fondrk, K., and Amdam, G. V. (2007) Immunogold localization of vitellogenin in the ovaries, hypopharyngeal glands and head fat bodies of honeybee workers, *Apis mellifera*. *J. Insect. Sci.* **7,** 1–14
34. Thapa, A., Shahnawaz, M., Karki, P., Raj Dahal, G., Sharoar, M. G., Yub Shin, S., Sup Lee, J., Cho, B., and Park, I. S. (2008) Purification of inclusion body-forming peptides and proteins in soluble form by fusion to *Escherichia coli* thermostable proteins. *BioTechniques* **44,** 787–796
35. Fischer, H. D., Gonzalez-Noriega, A., and Sly, W. S. (1980) β-Glucuronidase binding to human fibroblast membrane receptors. *J. Biol. Chem.* **255,** 5069–5074
36. Kirankumar, N., Ismail, S. M., and DuttaGupta, A. (1997) Uptake of storage protein in the rice moth *Corcyra cephalonica*. Identification of storage protein binding proteins in the fat body cell membranes. *Insect Biochem. Mol. Biol.* **27,** 671–679
37. Tong, Z., Li, L., Pawar, R., and Zhang, S. (2010) Vitellogenin is an acute phase protein with bacterial-binding and inhibiting activities. *Immunobiology* **215,** 898–902
38. Fiske, C. H., and Subbarow, Y. (1925) The colorimetric determination of phosphorus. *J. Biol. Chem.* **66,** 374–389
39. Anderson, T. A., Levitt, D. G., and Banaszak, L. J. (1998) The structural basis of lipid interactions in lipovitellin, a soluble lipoprotein. *Structure* **6,** 895–909
40. Raag, R., Appelt, K., Xuong, N. H., and Banaszak, L. (1988) Structure of the lamprey yolk lipid-protein complex lipovitellin-phosvitin at 2.8 Å resolution. *J. Mol. Biol.* **200,** 553–569
41. Lehtonen, J. V., Still, D. J., Rantanen, V. V., Ekholm, J., Björklund, D., Iftikhar, Z., Huhtala, M., Repo, S., Jussila, A., Jaakkola, J., Pentikäinen, O., Nyrönen, T., Salminen, T., Gyllenberg, M., and Johnson, M. S. (2004) BODIL. A molecular modeling environment for structure-function analysis and drug design. *J. Comput. Aided Mol. Des.* **18,** 401–419
42. Avarre, J. C., Lubzens, E., and Babin, P. J. (2007) Apolipocrustacein, formerly vitellogenin, is the major egg yolk precursor protein in decapod crustaceans and is homologous to insect apolipophorin II/I and vertebrate apolipoprotein B. *BMC Evol. Biol.* **7,** 3
43. Jones, D. T. (1999) Protein secondary structure prediction based on position-specific scoring matrices. *J. Mol. Biol.* **292,** 195–202
44. Marheineke, K., Grünewald, S., Christie, W., and Reiländer, H. (1998)

Lipid composition of *Spodoptera frugiperda* (Sf9) and *Trichoplusia ni* (Tn) insect cells used for baculovirus infection. *FEBS Lett.* **441,** 49–52
45. Podack, E. R., Hengartner, H., and Lichtenheld, M. G. (1991) A central role of perforin in cytolysis? *Annu. Rev. Immunol.* **9,** 129–157
46. Kent, C. F., Issa, A., Bunting, A. C., and Zayed, A. (2011) Adaptive evolution of a key gene affecting queen and worker traits in the honey bee, *Apis mellifera*. *Mol. Ecol.* **20,** 5226–5235
47. Campanella, C., Caputo, M., Vaccaro, M. C., De Marco, N., Tretola, L., Romano, M., Prisco, M., Camardella, L., Flagiello, A., Carotenuto, R., Limatola, E., Polzonetti-Magni, A., and Infante, V. (2011) Lipovitellin constitutes the protein backbone of glycoproteins involved in sperm-egg interaction in the amphibian *Discoglossus pictus*. *Mol. Reprod. Dev.* **78,** 161–171
48. Havukainen, H., Halskau, Ø., and Amdam, G. V. (2011) Social pleiotropy and the molecular evolution of honey bee vitellogenin. *Mol. Ecol.* **20,** 5111–5113
49. Wickman, G., Julian, L., and Olson, M. F. (2012) How apoptotic cells aid in the removal of their own cold dead bodies. *Cell Death Differ.* **19,** 735–742
50. Cocca, B. A., Cline, A. M., and Radic, M. Z. (2002) Blebs and apoptotic bodies are B cell autoantigens. *J. Immunol.* **169,** 159–166
51. Tait, J. F., Gibson, D. F., and Smith, C. (2004) Measurement of the affinity and cooperativity of annexin V-membrane binding under conditions of low membrane occupancy. *Anal. Biochem.* **329,** 112–119
52. Balasubramanian, K., Chandra, J., and Schroit, A. J. (1997) Immune clearance of phosphatidylserine-expressing cells by phagocytes. The role of β2-glycoprotein I in macrophage recognition. *J. Biol. Chem.* **272,** 31113–31117
53. Bottazzi, B., Doni, A., Garlanda, C., and Mantovani, A. (2010) An integrated view of humoral innate immunity. Pentraxins as a paradigm. *Annu. Rev. Immunol.* **28,** 157–183
54. Cocca, B. A., Seal, S. N., D'Agnillo, P., Mueller, Y. M., Katsikis, P. D., Rauch, J., Weigert, M., and Radic, M. Z. (2001) Structural basis for autoantibody recognition of phosphatidylserine-β2 glycoprotein I and apoptotic cells. *Proc. Natl. Acad. Sci. U.S.A.* **98,** 13826–13831
55. Montaville, P., Neumann, J. M., Russo-Marie, F., Ochsenbein, F., and Sanson, A. (2002) A new consensus sequence for phosphatidylserine recognition by annexins. *J. Biol. Chem.* **277,** 24684–24693
56. Gasparovic, A. C., Jaganjac, M., Mihaljevic, B., Sunjic, S. B., and Zarkovic, N. (2013) Assays for the measurement of lipid peroxidation. *Methods Mol. Biol.* **965,** 283–296
57. Reuter, S., Gupta, S. C., Chaturvedi, M. M., and Aggarwal, B. B. (2010) Oxidative stress, inflammation, and cancer. How are they linked? *Free Radic. Biol. Med.* **49,** 1603–1616
58. Tilg, H., and Moschen, A. R. (2006) Adipocytokines. Mediators linking adipose tissue, inflammation and immunity. *Nat. Rev. Immunol.* **6,** 772–783
59. Amdam, G. V., Hartfelder, K., Norberg, K., Hagen, A., and Omholt, S. W. (2004) Altered physiology in worker honey bees (Hymenoptera: Apidae) infested with the mite Varroa destructor (Acari: Varroidae). A factor in colony loss during overwintering? *J. Econ. Entomol.* **97,** 741–747
60. Amdam, G. V., Norberg, K., Hagen, A., and Omholt, S. W. (2003) Social exploitation of vitellogenin. *Proc. Natl. Acad. Sci. U.S.A.* **100,** 1799–1802
61. Amdam, G. V., Simões, Z. L., Guidugli, K. R., Norberg, K., and Omholt, S. W. (2003) Disruption of vitellogenin gene function in adult honeybees by intra-abdominal injection of double-stranded RNA. *BMC Biotechnol.* **3,** 1
62. Münch, D., and Amdam, G. V. (2010) The curious case of aging plasticity in honey bees. *FEBS Lett.* **584,** 2496–2503